



# Structure and composition of $\text{Ba}_{0.5}\text{Sr}_{0.5}\text{TiO}_3$ films deposited on (001) MgO substrates and the influence of sputtering pressure

M.E. Twigg\*, L.M.B. Alldredge, W. Chang, A. Podpirka, S.W. Kirchoefer, J.M. Pond

Electronics Science and Technology Division, Naval Research Laboratory, Washington DC 20375, USA

## ARTICLE INFO

### Article history:

Received 19 February 2013

Received in revised form 16 September 2013

Accepted 18 September 2013

Available online 25 September 2013

### Keywords:

Transmission electron microscopy

Barium strontium titanate

Stacking faults

Dislocations

Sputter deposition

Ruddlesden–Popper faults

## ABSTRACT

The structure and composition of  $\text{Ba}_{0.5}\text{Sr}_{0.5}\text{TiO}_3$  thin films, sputter deposited on (001) MgO substrates, have been characterized by transmission electron microscopy. Deviations in film stoichiometry are seen to strongly correlate with the structural and dielectric properties of these films, with the films deposited at the lower sputtering pressures either Ti-deficient or capped with a titanium oxide layer similar to the rutile  $\text{TiO}_2$  phase. Preferential sputtering of cations is found to be an important factor governing film stoichiometry. The Ti-deficient films deposited at a lower sputtering pressure contain Ruddlesden–Popper faults that increase the average lattice constant of the film and result in compressive strain and low dielectric tunability.

Published by Elsevier B.V.

## 1. Introduction

Ferroelectric films of the perovskite structure  $\text{ABO}_3$ , such as  $\text{Ba}_{1-x}\text{Sr}_x\text{TiO}_3$  (BST) ( $0 < x < 1$ ), are of particular interest due to the material's high dielectric permittivity and tunability [1,2], both of which depend on the strain state of the film [3]. For sputter-deposited BST films grown on (001) MgO substrates, the film cation composition, as well as the resulting strain state determined by X-ray diffraction, are strongly dependent on the sputtering pressure maintained over the course of film deposition [1,4]. Films under slight compression or slight tension are expected to exhibit the highest tunability (measured by interdigitated electrodes applying a lateral electric field) [5,6], in accordance with Landau–Ginzburg–Devonshire free energy density function theory [7–10]. For a film under large compressive strain, lateral ionic motion is restricted (especially that of Ti), thereby inhibiting dielectric tunability. For a film under tension or only slight compression, lateral ionic motion is less heavily constrained, thus allowing the dielectric properties to be altered by the application of a lateral electric field.

The chemical diffusivities of atoms in perovskites are seen to increase with decreasing oxygen partial pressure, resulting in quickly diffusing oxygen vacancies that give rise to chemical potentials that drive, in turn, the comparatively slowly-diffusing cations [11]. As a consequence, diffusion-driven cation non-stoichiometry in BST films occurs when these films are deposited at lower oxygen partial pressures. The oxygen and cation vacancy concentrations also influence the generation of extended defects that, together with film composition, influence the strain state of the film and its dielectric properties. In this paper,

transmission electron microscopy (TEM) is used to determine film structure, composition, and extended defect type and concentration, in sputter-deposited BST films grown on (001) MgO substrates over a range of sputtering pressures and argon to oxygen ratios. These observations, in turn, lead to a better understanding of the sputtered growth and dielectric properties of these films.

## 2. Experimental details

The BST ( $x = 0.5$ ) films in this study were deposited onto (001) MgO substrates (cubic, lattice parameter 0.4212 nm) by radio frequency magnetron sputtering using conditions similar to those described previously [4]. The target size was 3 in. in diameter and all five films were deposited using 90 W of power. Three films were deposited using an Ar:O<sub>2</sub> ratio of 1:2; two at a sputtering pressure of 6.7 Pa and one at a sputtering pressure of 30 Pa (corresponding to oxygen partial pressures of 4.4 and 20 Pa, respectively). One film was deposited with an Ar:O<sub>2</sub> ratio of 2:1, where the sputtering pressure was 27 Pa and the oxygen partial pressure 8.9 Pa. The outlier of the group was a film deposited with an Ar:O<sub>2</sub> ratio of 18:1 and a total pressure of 1.3 Pa (corresponding to an oxygen partial pressure of 0.07 Pa). In most cases, we will refer to these samples by the sputtering pressure. For all five films, the substrate was held at 825 °C during deposition. A post-deposition anneal of each film was performed at 950 °C for 6 h in flowing O<sub>2</sub>.

The strain state of each BST film was determined via X-ray diffraction. Table 1 lists the ambient temperature values of the in-plane lattice parameter  $a$ , and the out-of-plane BST lattice parameter  $c$ , for each BST film. The value of  $a$  was determined from the asymmetric in-plane (024)  $\theta$ – $2\theta$  reflection and the value of  $c$  was determined from the

\* Corresponding author.

**Table 1**  
BST parameters as a function of sputtering pressure.

p (Pa)	pO <sub>2</sub> (Pa)	t (nm)	a (nm)	c (nm)	a <sub>0</sub> (nm)	( $\Delta a/a$ ) <sub>in</sub> (%)	$\epsilon_r$	Loss (%)	Tuning (%)
1.3	0.07	360	0.3965	0.3982	0.3974	−0.29	131	0.04	4.7
6.7	4.4	320	0.3880	0.4004	0.3945	−2.12	363	0.06	17
6.7	4.4	450	0.3895	0.3996	0.3948	−1.73	177	0.07	18
27	8.9	310	0.3949	0.3965	0.3957	−0.28	560	0.14	48
30	20	210	0.3961	0.3960	0.3960	+0.01	534	0.11	44

symmetric out-of-plane (004)  $\theta$ – $2\theta$  reflection, while using the MgO substrate as a reference. The in-plane strain  $(\Delta a/a)_{in} = (a - a_0) / a_0$  is given for each sample in Table 1, where  $a_0$  is the freestanding lattice constant of the film calculated from  $a_0 = [c + 2(c_{12}/c_{11})a]/[1 + 2(c_{12}/c_{11})]$ , where  $a$  and  $c$  are the in-plane and out-of-plane lattice parameters, respectively, and  $c_{11}$  and  $c_{12}$  are the elastic constants for BST ( $x = 0.5$ ) [4]. The dielectric measurements listed in Table 1 were performed at ambient temperature, with the relative dielectric permittivity  $\epsilon_r$  and loss tangent measured at 10 GHz and 0 V, and the dielectric tunability measured at 40 V, using a planar interdigitated capacitor structure applying a lateral electric field and conformal mapping to extract the film parameters. Each sample was prepared for Cross-sectional TEM (XTEM) using angle lapping and liquid nitrogen temperature argon ion milling. The sample grown at 1.3 Pa, which was prepared for Plan-View TEM (PVTEM), was thinned using only mechanical angle lapping. A Hitachi H9000UHR electron microscope operating at 300 kV was used to record Dark Field (DF) TEM images, High-Resolution TEM (HRTEM) images, and diffraction patterns from the XTEM and PVTEM samples. A JEOL 2200FS TEM was used for Energy Dispersive X-ray Spectroscopy (EDXS) of each XTEM sample in order to determine the composition of the BST layer.

### 3. Results

As shown in Table 1, BST films deposited at the relatively low sputtering pressure of 6.7 Pa have low dielectric loss, but poor tunability, while films deposited at the higher pressures of 27 Pa and 30 Pa have higher loss and good tunability [4]. The strain state of the 6.7–30 Pa films, from strongly compressive at 6.7 Pa to slightly tensile at 30 Pa, is seen to change monotonically as a function of sputtering pressure. The film grown at the lowest sputtering pressure of 1.3 Pa and a corresponding pO<sub>2</sub> value of 0.07 Pa, however, is only slightly compressively strained, and therefore falls outside of this trend. In order to understand the structural differences between these five films that lead to their different strain states, it is useful to begin with DF XTEM observations that reveal extended defects. Figs. 1–3 correspond to the BST films grown at values of 1.3, 6.7, and 27 Pa, respectively. For Figs. 1a–3a (Figs. 1b–3b) each DF XTEM image was recorded using a  $g = 020$  ( $g = 002$ ) diffraction vector. For the case of the 6.7 Pa sample, the XTEM images are taken from the 320 nm thick film. DF XTEM images of the 450 nm thick 6.7 Pa film and the 30 Pa film were also recorded and studied, but are not shown.

DF XTEM observations using the  $g = 020$  reflection show that each BST film is a textured single crystal consisting of 20–200 nm grains bounded by threading edge dislocations (TEDs) with densities on the order of  $10^{10}$ – $10^{11}/\text{cm}^2$  (Figs. 1a–3a). The grain size in the film grown at 1.3 Pa ranges from 20 to 50 nm (Fig. 1a). For the 6.7 Pa film (Fig. 2a), 27 Pa film (Fig. 3a), and 30 Pa film (not shown) the grain size ranges from 100 to 200 nm. The 6.7, 27, and 30 Pa films have a TED density on the order of  $10^{10}/\text{cm}^2$ . The 1.3 Pa film has a TED density on the order of  $10^{11}/\text{cm}^2$ , which correlates with its smaller grain size. This high density of TEDs is not unexpected for heteroepitaxial growth where the lattice mismatch between the film and substrate assumes the large value of  $-5.75\%$  for BST on MgO.

The threading screw dislocation (TSD) density in these films can be assessed from DF XTEM images recorded using the  $g = 002$  reflection,

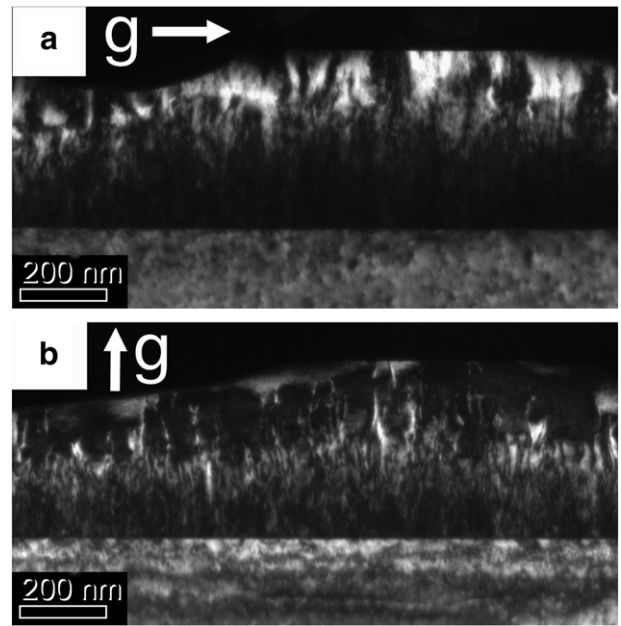


Fig. 1. DF XTEM of 1.3 Pa BST film: (a) for  $g = 020$ ; and (b) for  $g = 002$ .

as shown in Figs. 1b–3b. Despite the large lattice mismatch, however, the density of TSDs falls below the XTEM detectability limit of  $10^7/\text{cm}^2$  for the 6.7 Pa films, as seen in Fig. 2b. DF XTEM also reveals that the 6.7 Pa films contain planar defects, on the order of 10–20 nm in lateral extent, that are revealed by both  $g = 002$  and  $g = 020$  reflections. Higher magnification DF XTEM images that reveal more of the details of the lateral features are shown in Fig. 4a and b for the  $g = 002$  and  $g = 020$  reflections, respectively. HRTEM images of these features are consistent with Ruddlesden–Popper Faults (RPFs) [12], as shown in the HRTEM/XTEM image for the 6.7 Pa film in Fig. 5. The low density of TSDs in the 6.7 Pa films suggest that RPFs interfere with the propagation of TSDs, since TSD densities are on the order of  $10^{10}/\text{cm}^2$  in the RPF-free films grown at 27 and 30 Pa. For the case of the 1.3 Pa film, which is also RPF-free, the TSD density assumes a value on the order of  $10^{11}/\text{cm}^2$ .

Unlike the other four samples, the 1.3 Pa BST layer is capped by a 40–60 nm titanium oxide layer, as shown in Fig. 6. XTEM-based EDXS

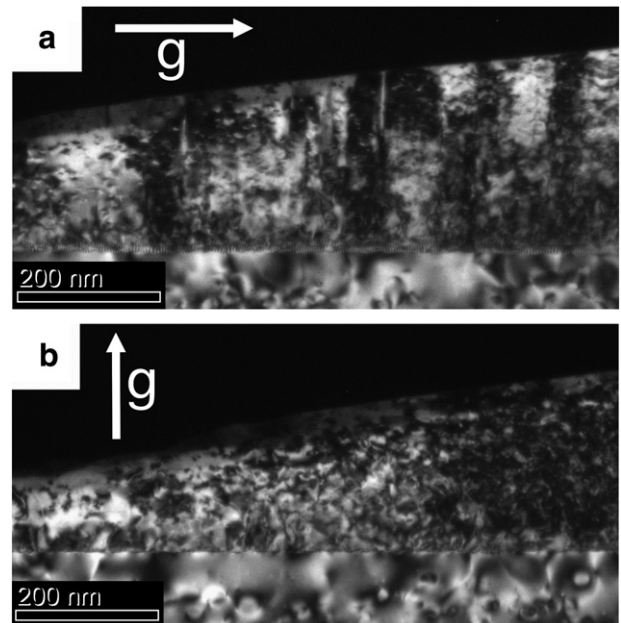


Fig. 2. DF XTEM of 6.7 Pa, 320 nm thick, BST film: (a) for  $g = 020$ ; and (b) for  $g = 002$ .

Download English Version:

<https://daneshyari.com/en/article/1665801>

Download Persian Version:

<https://daneshyari.com/article/1665801>

[Daneshyari.com](https://daneshyari.com)